Clinical Phytoscience

RESEARCH

Open Access

Green therapeutics' bio-AgNPs: a sustainable solution for multidrug-resistant pathogens

Nermine Mohammad Aboelnasr[1,2], Mohammed Abu-Elghait[3], Hassan M. Gebreel[1] and HebatAllah I. Youssef[1*]

Abstract

The escalating crisis of lethal multidrug resistance (MDR) pathogens and the alarming rise of resistance to last-resort antibiotics necessitate urgent exploration of innovative green therapeutic solutions. This study investigates the biogenic synthesis of silver nanoparticles (AgNPs) utilizing aqueous leaf extract from *Moringa oleifera* (MO) and evaluates their antibacterial efficacy against Gram-negative nosocomial pathogens. Among 150 nosocomial isolates, 3% demonstrated susceptibility to all tested antibiotics, underscoring the severity of the resistance dilemma. The antibacterial potential of the synthesized MO-AgNPs was assessed alongside their cytotoxic effects on a normal mouse liver cell line (BNL). The biosynthesis process involved the reduction of silver nitrate to silver using the MO leaf extract. Comprehensive characterization techniques—including UV-Vis spectroscopy, Fourier Transform Infrared (FTIR) spectroscopy, Zeta potential analysis, Dynamic Light Scattering (DLS), X-ray Diffraction (XRD), Scanning Electron Microscopy with Energy Dispersive X-ray (SEM-EDX), and Transmission Electron Microscopy (TEM) confirmed the formation of spherical MO-AgNPs with an average crystalline size of 12.89 nm. Antibacterial activity was evaluated via the broth microdilution method, revealing that MO-AgNPs exhibited bactericidal effects at a minimum inhibitory concentration (MIC) of ≤ 8 µg/mL for 80% of the pathogens, including 62% of difficult-to-treat (DTR) pathogens and over 90% among antibiotic class resistant groups, including colistin (Col R), extended-spectrum cephalosporins (ECR), fluoroquinolones (FQR), and carbapenems (CR). Importantly, these MICs remained below the cytotoxic threshold (IC_{50} = 13.47 µg/mL). These findings highlight the potential of biosynthesized MO-AgNPs as a novel broad-spectrum antibacterial agent, presenting a promising green therapeutic strategy to combat resistant bacterial infections.

Keywords *Moringa oleifera*, Multiple drug resistance, Difficult-to-treat resistance (DTR), Cytotoxicity, Biogenic AgNPs, Green therapeutic strategies, Reserve antibiotics, Colistin resistance

*Correspondence:
HebatAllah I. Youssef
hoba83@sci.asu.edu.eg
[1]Department of Microbiology, Faculty of Science, Ain Shams University, El-Khalyfa El-Mamoun Street Abbasya, Cairo, Egypt
[2]Basic Medical Sciences Department, Faculty of Oral and Dental Medicine, Misr International University, Cairo, Egypt
[3]Department of Botany and Microbiology, Faculty of Science, Al-Azhar University, Cairo, Egypt

Introduction

Over the past twenty years, antimicrobial resistance has escalated globally, affecting treatment efficiency and increasing mortality rates [1]. In 2021, the World Health Organization estimated that mortality rates would reach 10 million annually by 2050 [2]. Due to the lack of effective antibiotics, Colistin was revived and used as the last resort antibiotic. Unfortunately, the alarming rise in resistance to colistin has been reported [3], which requires the exploration of new therapeutic alternatives. Bio-nanotechnology is one of the green therapeutic approaches that actively contributes to the fabrication of innovative, sustainable anti-microbial drugs with novel modes of action, which are essential in combating these lethal superbugs [4].

Silver nanoparticles (AgNPs) have garnered attention for their therapeutic properties especially their potent antimicrobial activity and lower toxicity compared to other nanoparticles [5]. Traditional synthesis methods for AgNPs, such as chemical reduction and electrochemical techniques, often involve hazardous chemicals and high costs, raising environmental concerns. In contrast, green biosynthesis utilizing plant extracts offers a sustainable and eco-friendly alternative, leveraging secondary metabolites as reducing and stabilizing agents [6].

Moringa oleifera (MO) is a woody tree that grows in tropical and subtropical areas of Asia, Africa, and the Middle East. Traditionally, MO has been used to cure skin conditions, hypertension, diabetes, parasitic infections, and malaria. Pharmacological characteristics of MO is rich in antioxidant, anti-inflammatory, anti-cancer, anti-hyperglycemic, and anti-hyperlipidemic [7]. Owing to its exceptional nutritional and therapeutic properties. it is referred to as a "nature gift", the "Miracle Tree" or the "Tree of Life" [8]. MO has drawn attention as an eco-friendly tool for the biogenic production of diverse nanoparticles owing to its diverse array of secondary metabolites [9, 10].

Despite the promising antibacterial properties of green-synthesized AgNPs, research remains limited, particularly concerning their efficacy against nosocomial pathogens, which are often more resistant than standard laboratory strains. This study aims to biogenically synthesize AgNPs using MO aqueous leaf extract and evaluate their antimicrobial properties among drug-resistant phenotypes of nosocomial pathogens with a focus on emerging classification approaches for Multi-drug resistance (MDR) phenotypes, including the usual drug resistance (UDR), Difficult-to-treat resistance (DTR), and Center of Disease Control's antibiotic-class resistance categories; Carbapenem resistance (CR), Extended-spectrum cephalosporin resistance (ECR), and Fluoroquinolone resistance (FQR), along with evaluation of reserve antibiotic resistance (last resort antibiotics) including Colistin (Col), Tigecycline (TGC), and Ceftazidime-avibactam (CZA). In addition, the cytotoxic effect on a normal mouse liver cell line (BNL) was evaluated to explore the potential of MO-AgNPs as a novel therapeutic alternative.

Materials and methods

Isolates collection

Non-duplicate Gram-negative bacilli (GNB) isolates were collected from the Microbiology labs of four Egyptian hospitals: International Medical Center (IMC), Dar Al-Fouad Hospital (DAF), Ain Shams University (ASU), and Mansoura University Hospital (MU). Isolates were collected from inpatients admitted to different health care units (ICU and non-ICU) over 8 months from May 2021 to December 2021. The patient's demographics were recorded (gender, location, specimen, and type of infection). The collected isolates were from Blood, Urine, Sputum, Wound swabs, Stool, and Cerebrospinal fluid (CSF). Identification and Susceptibility testing were carried out using Biomérieux VITEK® 2 system on different antibiotics including Ampicillin (AMP), ampicillin/clavulanic (AMC), piperacillin/tazobactam (TZP), Cefazolin (CZ), Cefoxitin (FOX), Ceftazidime (CAZ), Cefotaxime (CTX), Ceftriaxone (CRO), Ceftazidime/avibactam (CZA), Cefepime (CPM), imipenem (IPM), meropenem (MEM), gentamicin (GN), levofloxacin (LEV), ciprofloxacin (CIP), tigecycline (TGC) and trimethoprim/sulfamethoxazole (SXT). Susceptibility results interpretation was done according to Clinical Laboratory Standards Institute (CLSI) recommendations [11]. Susceptibility to Colistin (COL) was confirmed by the broth microdilution method (BMD) [12].

Definitions of drug-resistance phenotypes and antibiotic-class resistance

In this study, the isolated GNB were classified into three phenotypes: Susceptible (S), UDR, and DTR isolates. Susceptible isolates were described as sensitive to all antibiotics except those with intrinsic resistance. UDR was described as non-intrinsic in vitro resistance or intermediate to one or more antibiotics, but still effectively treated with first-line antibiotics [13]. DTR was described as non-intrinsic resistance or intermediate resistance in vitro to all first-line antibiotics, the β-lactam categories, among which are carbapenems and fluoroquinolones [14]. Furthermore, antibiotic class resistance was categorized according to the Centers of Disease Control (CDC) definitions [15]. CR was identified as the in vitro resistance to imipenem and meropenem. Ceftazidime, cefotaxime, and cefepime resistance in vitro were characterized as ECR. The in vitro resistance to ciprofloxacin and levofloxacin was identified as FQR. [16–18].

M. Oleifera leaves extract preparation

Fresh leaves of *Moringa oleifera* (MO), (Family: *Moringaceae*) were obtained from the Horticulture Research Institute, Agriculture Research Center in Cairo. The leaves were washed and air-dried. 10 g of MO dried leaves fine powder was added to 100 mL of double-distilled water, then heated at 100 °C for 30 minutes. The extract was filtered using filter paper (Whatman no. 1) and stored at 4 °C [6].

Biogenic silver nanoparticles preparation

Using Silver nitrate ($AgNO_3$) as a precursor, a 2 mM solution of $AgNO_3$ was prepared using double-distilled water and stored in a dark bottle. 10 mL of MO leaves extract was added dropwise into 90 mL of 2 mM aqueous solution of $AgNO_3$ and heated with continuous stirring at 60 °C for 1 h [19]. The color shift from yellow to reddish brown indicated the formation of AgNPs, as shown in Fig. 1. The solution was centrifuged for 20 minutes at 15,000 rpm. After discarding the supernatant, the pellet was washed three times with distilled water for 10 minutes each. Then, the pellet was heated to dryness at 100

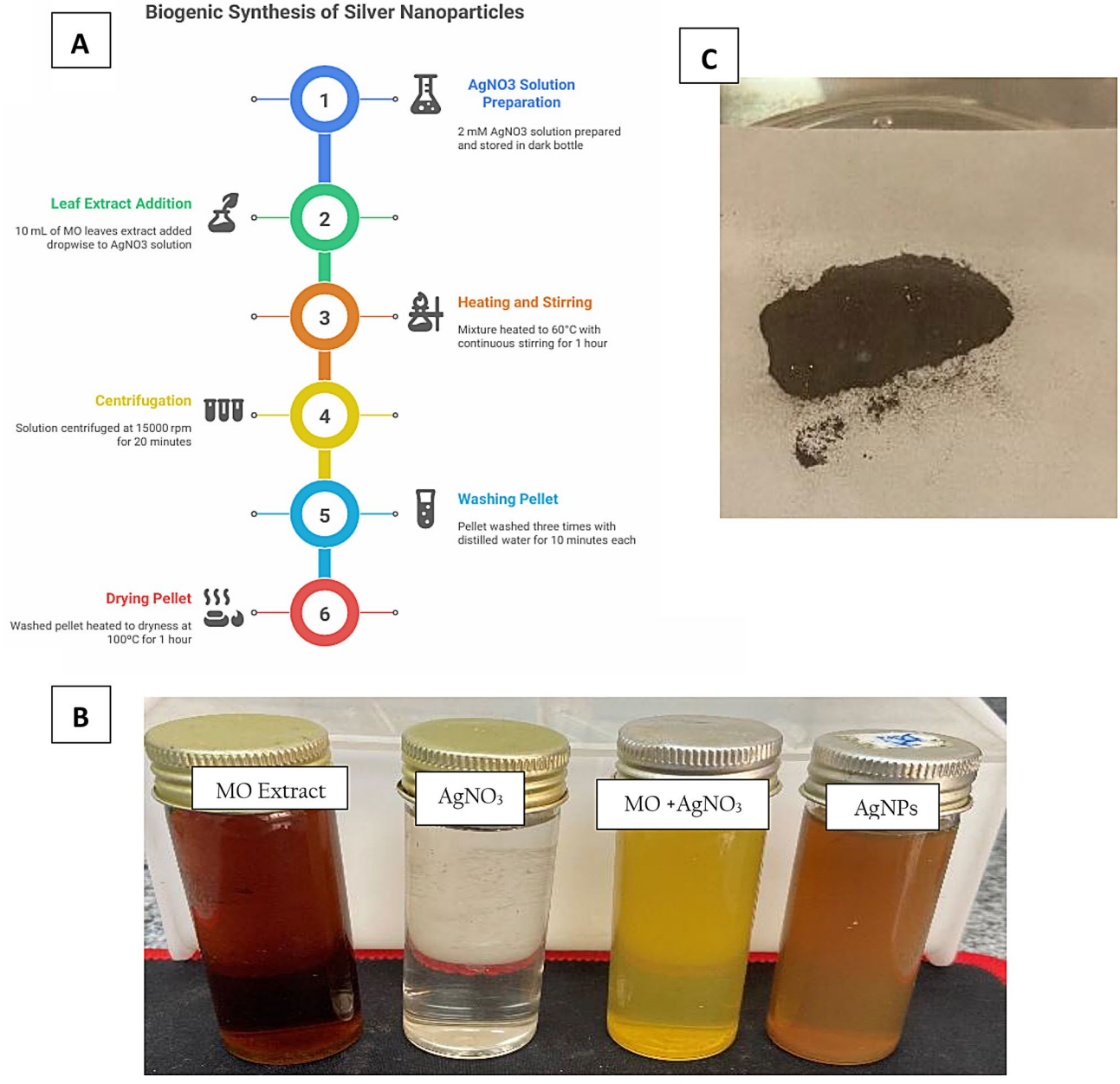

Fig. 1 (**A**) Schematic diagram for biogenic synthesis of silver nanoparticles from Moringa Oleifera leave extract (**B**) Moringa leaves extract, silver nitrate solution, reaction mixture "yellow color", end-product reddish brown color, and (**C**) the black powder after drying (MO-AgNPs)

°C for 1 hour. Finally, MO-AgNP powder was collected as shown in Fig. 1.

Characterization of MO-AgNPs

UV-VIS spectroscopy (Shimadzu, UV-1800, Japan) was used to measure the surface plasmon resonance band after the color changed from yellow to reddish-brown, indicating the synthesis of AgNps [20]. The functional groups of the organic compounds in the MO that capped the AgNPs (MO-AgNPs) were identified using Fourier transformation infrared (FTIR) spectroscopy (Vertex 70 FTIR spectrometer, Bruker Optik GmbH). SEM-EDX analysis (*ZEISS* Smart SEM-EDX, Germany) was used for visualization of the shape of silver nanoparticles, and elemental composition identification of the biogenic nanoparticles. The hydrodynamic size and zeta potential of the biogenic MO-AgNPs were measured by Dynamic light scattering (DLS) (Litesizer 500, Anton Paar, USA). An X-ray powder diffractometer (Shimadzu XRD-6000, Japan) was used to determine the structural analysis of the synthesized MO-AgNPs. XRD patterns are obtained in the range of 2θ from 4° to 90° at room temperature. The MO-AgNPs crystalline size was calculated using Scherrer's equation:

$$D = \frac{K\lambda}{\beta \cos(\theta)}$$

Where D is the average crystallite size, K is the shape factor (typically taken as 0.9), λ is the wavelength of the X-ray radiation (λ = 1.5406 Å), β is the full width at half maximum (FWHM) of the diffraction peak in radians, and θ is the diffraction angle [21–23].

Transmission microscope (JEM 100CX, JEOL, Japan) imaging determined the shape and measured the size of the synthesized nanoparticles.

Antibacterial analysis of MO-AgNPs

Antimicrobial criteria were evaluated by the broth microdilution method (BMD). In brief, BMD was performed using two-fold serial dilutions of MO-AgNPs and cation-adjusted Muller Hinton broth (CaMHB, Condalab, Spain). MO-AgNP concentrations ranging from 2 to 256 µg/mL were prepared in double-distilled water from a stock solution (1 mg/mL), followed by sterilization by UV exposure for 1 h to eliminate any undesirable contamination [6]. A standardized inoculum of 0.5 McFarland (1.5 x10^4 CFU/well) was prepared. 50 µL of MO-AgNPs of each concentration were added to 50 µL of inoculum in each well. The final concentrations of MO-AgNPs/well were:128 µg/mL, 64 µg/mL, 32 µg/mL, 16 µg/mL, 8 µg/mL, 4 µg/mL, 2 µg/mL, 1 µg/mL, 0.5 µg/mL, and 0.25 µg/mL. To determine MIC endpoints, the lowest concentration showing no visual bacterial growth was recorded as the Minimum inhibitory concentration (MIC) value after 24 h incubation. The MIC and the wells of higher concentrations were cultured on agar plates. The Minimum bactericidal concentration (MBC) value represented the lowest concentration of MO-AgNPs that showed no growth on the agar plates. The MBC/MIC ratio was calculated, and ratios equal to or below 4 were considered to have a bactericidal effect [24].

Cytotoxicity assay of MO-AgNPs using the MTT technique

The Normal mouse liver cell line (BNL) was purchased from Nawah Scientific, Inc. (Mokatam, Cairo, Egypt). Cell viability was assessed by 3-(4,5-dimethylthiazol-2-yl)-2,5- diphenyltetrazolium bromide (MTT) assay. 100 µL cell suspension (5x10^3 cells) was seeded in 96-well plates and incubated in complete media for 24 h at 37 °C in 5% CO_2. Cells were replenished with 100 µL media containing MO-AgNPs with concentrations (0.01, 0.03, 0.1, 0.3, 1, 3, 10, 30, 100, and 300 µg/mL) after 48 h of MO-AgNPs exposure, the media was discarded, and 20 µL of MTT solution was added along with 100 µL PBS in each well and incubated at 37 °C for 4 h. Finally, the plate was measured at λ_{max} 570 nm using a plate reader (BMG Labtech Fluo®star Omega, Germany). The experiment was performed in triplicates [25]. IC50 (half maximal inhibitory concentration) of MO-AgNPs was calculated according to the equation [19]:

$$\mathrm{IC50} = \frac{\mathrm{control\,OD} - \mathrm{sample\,OD}}{\mathrm{control\,OD}} \times 100$$

The dose-response curve was plotted using GraphPad Prism software.

Results

Isolation and identification of pathogens

Among a total of 150 non-duplicate nosocomial GNBs collected, 74 were *K. pneumoniae,* 35 were *E. coli,* 12 were *P. aeruginosa,* 14 were *A. baumannii,* 7 were *Proteus mirabilis* and 8 were other species (3 *Serratia marcescens*, 3 *Salmonella sp*., 1 *Citrobacter koseri,* and 1 *Sphingomonas paucimobis*).

Susceptibility patterns

Susceptibility testing results with MICs are shown in Table 1S. Susceptibility patterns revealed that only 3% (*n* = 4) of isolates were susceptible to all antibiotics (S), 53% (*n* = 80) were UDR, and 44% (*n* = 66) were DTR, Moreover, Antibiotic class resistance showed, 49% (*n* = 74) were CR, 63% (*n* = 95) were FQR, 75% (*n* = 113) were ECR and 79% (*n* = 118) were Col R. The Majority of *A. baumannii* were DTR isolates, with a prevalence rate of 86% (*n* = 12), unlike *P. mirabilis* and *E. coli*, which

Table 1 Distribution of drug-resistance phenotypes and antibiotic class-resistance among gnb of the study

	Acinetobacter baumannii (*n* = 14), N (%)	Klebsiella pneumoniae (*n* = 74), N (%)	E. coli (*n* = 35), N (%)	Pseudomonas aeruginosa (*n* = 12), N (%)	Proteus mirabilis (*n* = 7), N (%)	Others (*n* = 8), N (%)
Resistance categories						
S	0 (0%)	1 (1%)	1 (3%)	2 (17%)	0 (0%)	0 (0%)
UDR	2 (14%)	29 (39%)	30 (86%)	7 (58%)	5(86%)	7 (88%)
DTR	12 (86%)	44 (59%)	4 (11%)	3 (25%)	2 (29%)	1 (20%)
Antibiotic class resistance						
CR	12 (86%)	46 (62%)	6 (17%)	6 (50%)	3 (43%)	1 (13%)
ECR	12 (86%)	63 (85%)	26 (74%)	4 (33%)	4 (57%)	2 (25%)
FQR	14 (100%)	54 (73%)	17 (49%)	5 (42%)	5 (71%)	1 (13%)
Reserve antibiotic						
Col R	12 (86%)	59 (80%)	23 (66%)	9 (75%)	7 (100%)	5 (63%)
TGC R	9 (64%)	21 (28%)	1(3%)	3 (25%)	4(57%)	1 (20%)
CZA R	14 (100%)	56 (76%)	12 (34%)	6 (50%)	3 (43%)	2 (25%)

Abbreviations: S: susceptible; UDR: Usual drug resistance; CR, carbapenem resistance; DTR, difficult-to-treat resistance; ECR, extended-spectrum cephalosporin resistance; FQR, fluoroquinolone resistance; Col R: Colistin resistance; TGC R: tigecycline resistance, CZA R: Ceftazidime/avibactam

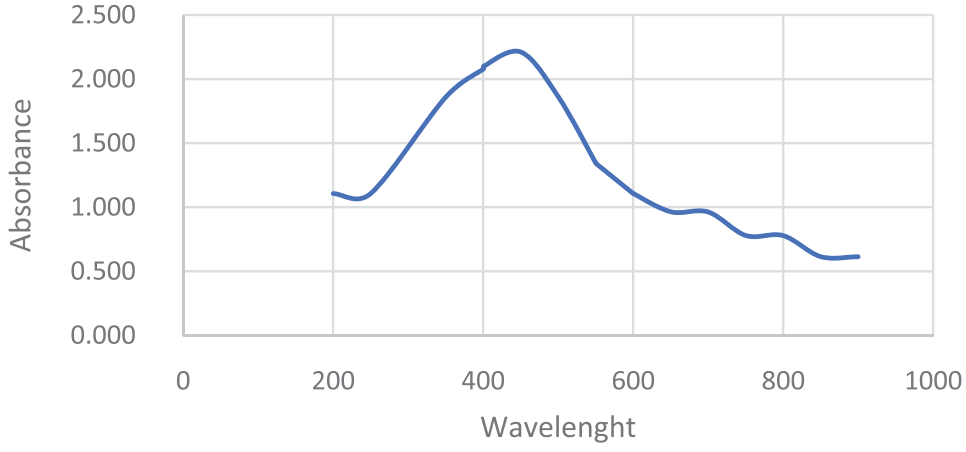

Fig. 2 UV-VIS spectroscopy results

exhibited the highest UDR phenotype, with prevalent rates of 86% each.

Resistance phenotypes per species

A. baumannii exhibited the highest CR, FQR, ECR, and Col R resistance phenotypes, accounting for 86% (*n* = 12) for each CR, FQR, and Col R, and 100% (*n* = 14) for ECR followed by K. pneumoniae, which accounted for 85% (*n* = 63) ECR, and 80% Col R. ECR was the most prevalent drug-resistant phenotype for E. coli., accounting for 74% (*n* = 26). For P. aeruginosa, Col R was the highest resistance phenotype, accounting for 75%. For Proteus mirabilis, FQR was the main resistant phenotype accounting for 71% (*n* = 5). Both S. marcescens and P. mirabilis are intrinsically resistant to colistin, as illustrated in Table 1.

Resistance to reserve antibiotics

Resistance to other Reserve antibiotics; Tigecycline (TGC) and Ceftazidime-avibactam (CZA) was reported in all tested pathogens and was elevated in *A. baumannii* and *K. pneumoniae* as illustrated in Table 1.

Infections

Regarding the data analysis of Infections in the study, Urinary tract infections (UTI) were the most prevalent, accounting for 36% (*n* = 54) of the total infections, followed by Respiratory tract infections (RTI) and Bloodstream infections (BSI) with percentages of 29% (*n* = 44) and 23% (*n* = 35), respectively. DTR pathogens predominated RTI, with percentages of 59% (*n* = 26), followed by BSI with percentages of 44% (*n* = 15) as shown in Figure 1S. ICU infections accounted for 64% (*n* = 96) of the total infections, out of which 56% (*n* = 54) were DTR infections.

Characterization of MO-AgNPs

UV–VIS absorption spectra analysis

The UV-vis spectra of the synthesized nanoparticles showed a surface plasmon resonance (SPR) peak at 450.7 nm, confirming the formation of AgNPs, as illustrated in Fig. 2. The SPR of AgNPs is responsible for the observed shift from a yellow to a reddish-brown in the

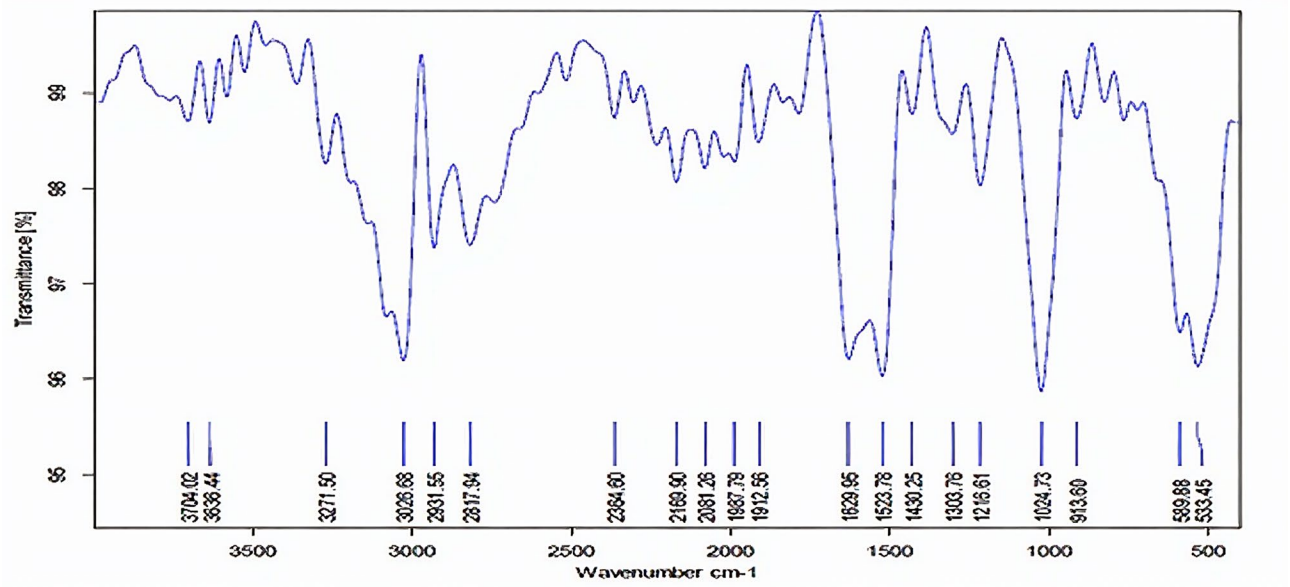

Fig. 3 FTIR spectra of MO-AgNPs

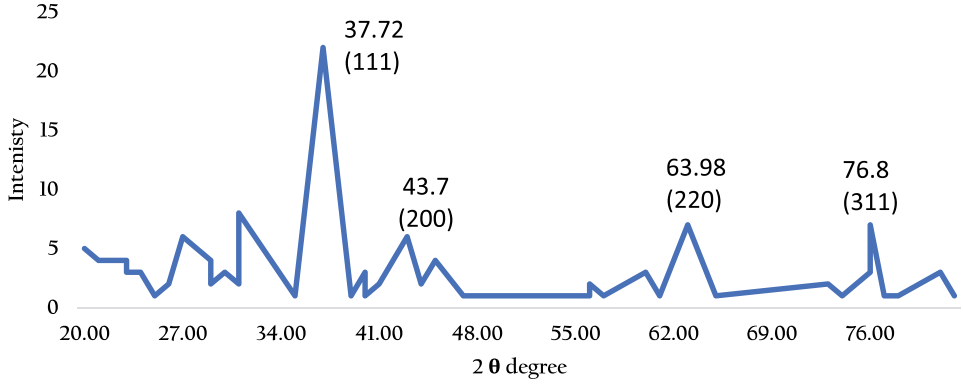

Fig. 4 X-ray diffraction spectra of the biosynthesized MO-AgNPs

aqueous solution because the free electrons in the metal are excited during the synthesis of AgNPs [20].

FT-IR analysis

As illustrated in Fig. 3, the FTIR analysis pattern showed that the broad absorption peak 3704.02 to 1912.56 cm^{-1} range can be assigned to hydroxyl (–OH) and amino (–NH) functional groups, suggesting that phytocompounds such as proteins and polysaccharides in the extract. The absorption peaks at 1629.95 and 1523.78 cm^{-1} are attributed to the stretching vibrations of carbonyl (C = O) groups and the bending vibrations of amino (N-H) groups, respectively, indicating the involvement of biomolecules like proteins in the synthesis process. Furthermore, the peaks in the 700 to 500 cm^{-1} region can attributed to the vibrational modes of metal-oxygen (M-O) bonds, suggesting linkages formation between the Ag ions and the functional groups of the phytocompounds of the MO leaf extract [26, 27]. Overall, the FTIR results provide evidence that phytocompounds are essential in the synthesis and stabilization of MO-AgNPs.

X-ray diffraction (XRD) analysis

XRD pattern showed four prominent diffraction peaks at 2 Theta angles 37°, 44°, 64° and 77°, as shown in Fig. 4. These 2 θ angles correspond to the 111, 200, 220, and 311 diffraction planes of the Face-Centered Cubic (FCC) structure of MO-AgNPs, respectively. The additional peaks indicate the presence of organic compounds linked to MO-AgNPs. Using Scherrer's formula, the calculated particle size was 12.89 nm [21–23]

Dynamic light scattering (DLS) and zeta potential analysis

DLS analysis showed that the average hydrodynamic size of MO-AgNPs is 120.28 nm. Figure 5a. The polydispersity index (PDI) was 19.4%, indicating that the particles are homogeneous in size, which can be beneficial for applications requiring consistent properties The mean zeta

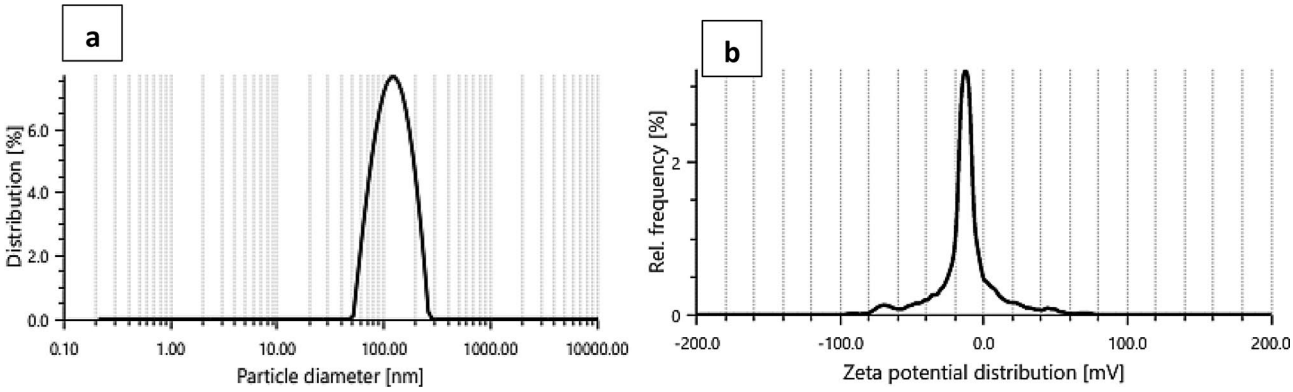

Fig. 5 (**a**) Dynamic light scattering (DLS) and (**b**) Zeta potential analysis for MO-AgNPs

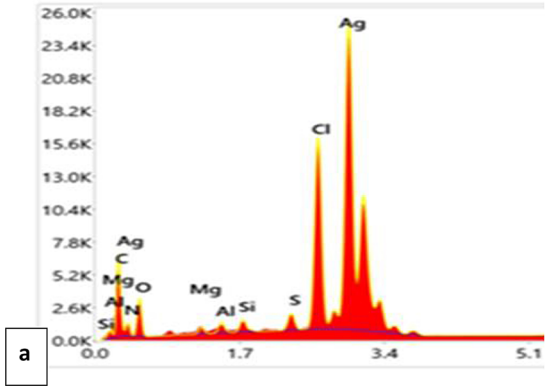

Element	Weight %	Atomic %
C	26.83	50.44
N	6.78	10.93
O	15.81	22.32
S	0.82	0.58
Cl	9.65	6.15
Ag	38.26	8.01

b

Fig. 6 EDX pattern of the synthesized MO-AgNPs (**a**), and (**b**) the weight and atomic percentages of the identified elements

potential of the biosynthesized MO-AgNPs is −13.3 mV, reflecting their electrostatic stability in suspension, Fig. 5b. The negative zeta potential indicates a negative surface charge on the nanoparticles, likely due to the presence of functional groups or ions on their surface [28].

SEM-EDX analysis

DX spectra, shown in Fig. 6, showed the elemental composition of the biogenic AgNPs; a strong silver signal and signals for other biomolecules, including C, N, O, S, and Cl. The EDX data provide the relative weight percentages and atomic percentages of the detected elements to assess the purity and composition of the biogenic MO-AgNPs. The high weight percent of Ag (38.26%) confirms the successful incorporation of Ag into the nanoparticles during the green synthesis process. The presence of carbon (C), nitrogen (N), and oxygen (O) in high weight and atomic percentages suggests the involvement of organic phytocompounds from the leaf extract in the synthesis and stabilization process, Fig. 6 SEM Imaging confirmed the spherical shape of the synthesized MO-AgNPs. The MO-AgNPs seem to have formed nanoclusters and aggregated together as shown in Figure 2S.

Transmission electron microscope (TEM)

The spherical morphology of MO-AgNPs was visualized by the Transmission Electron Microscope (TEM), and measured particle sizes ranged between 12.2 nm to 19.4 nm as shown in Fig. 7.

MO-AgNPs antibacterial activity

Broth microdilution results showed that most of the tested pathogens, 120 isolates (80%) scored a MIC ≤ 8 µg/mL, 40% ($n = 60$) scored MIC 4 µg/mL, and 20% ($n = 30$) scored MIC 16 µg/mL. The MBC/MIC ratio was below 4 in all isolates, demonstrating a bactericidal effect.

The MO-AgNPs MIC range in *A. baumannii* was 4–16 µg/mL, 0.25–16 µg/mL in *K. pneumoniae,* 0.25–4 µg/mL in *E. coli,* 2–8 µg/mL in *P. aeruginosa,* and 4 µg/mL in *P. mirabilis* as shown in Fig. 8

The MICs across drug-resistant phenotypes showed that 70% ($n = 19$) of DTR pathogens scored a MIC of 8 µg/mL, and 90% ($n = 9$) of UDRs scored a MIC of 2 µg/mL. MICs ≤ 8 µg/mL were reported in 62% ($n = 41$) of DTRs and 94% ($n = 75$) of UDR pathogens, as shown in Fig. 9.

The MIC of MO-AgNPs across antibiotic class resistances were ≤ 8 µg/mL in 98% ($n = 113$) of the Col R class, 96% ($n = 109$) in ECR, 94% ($n = 88$) in FQR, and 92% ($n = 68$) in CR as illustrated in Figures 10 & 3S.

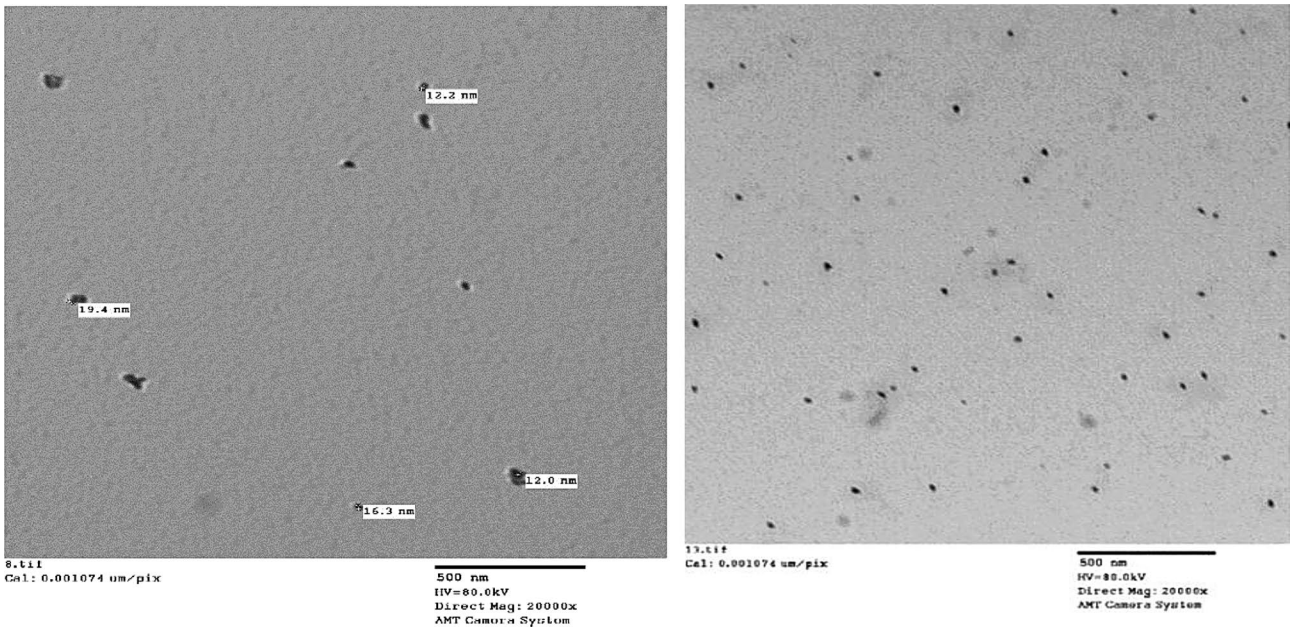

Fig. 7 TEM imaging of MO-AgNps

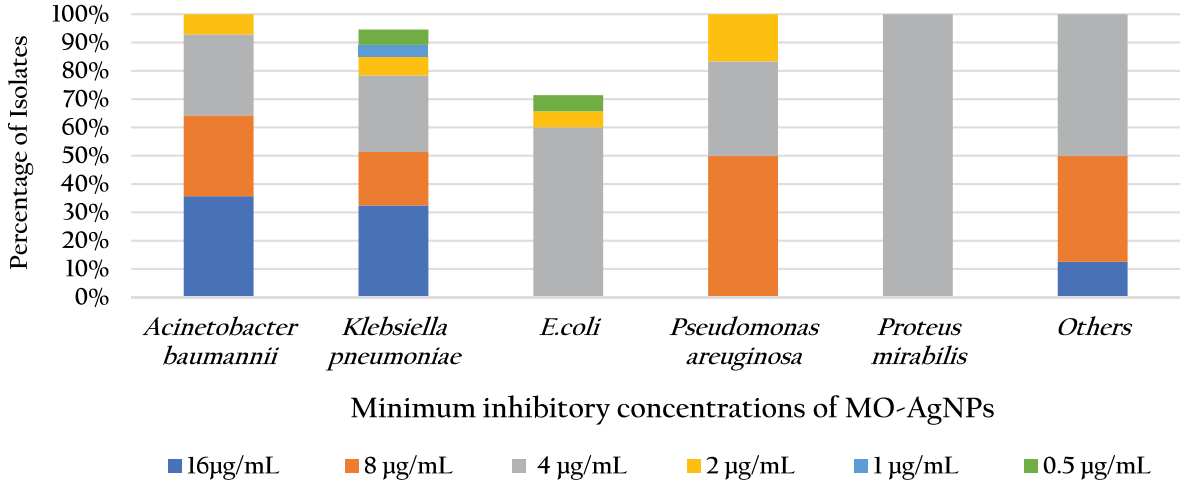

Fig. 8 Minimum inhibitory concentrations of MO-AgNPs against GNB pathogens

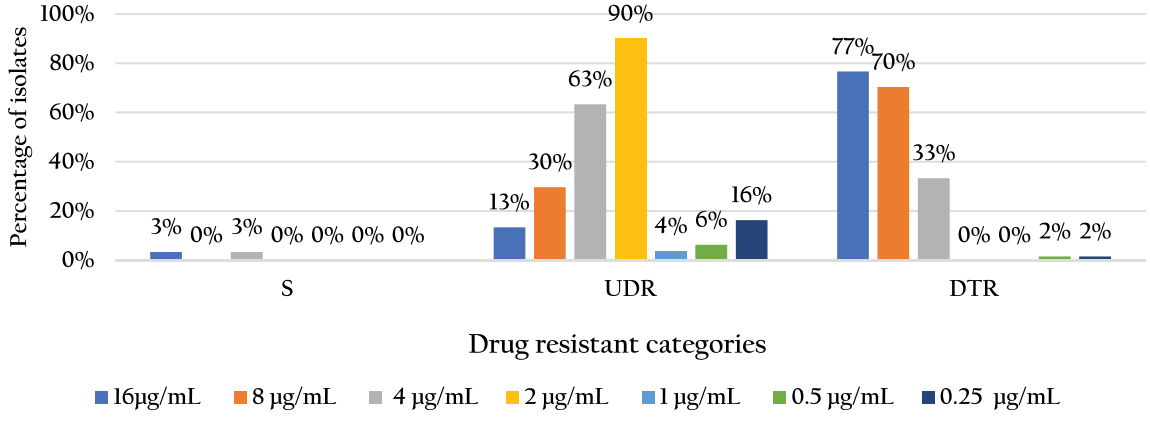

Fig. 9 Minimum inhibitory concentrations of MO-AgNPs across drug resistance phenotypes

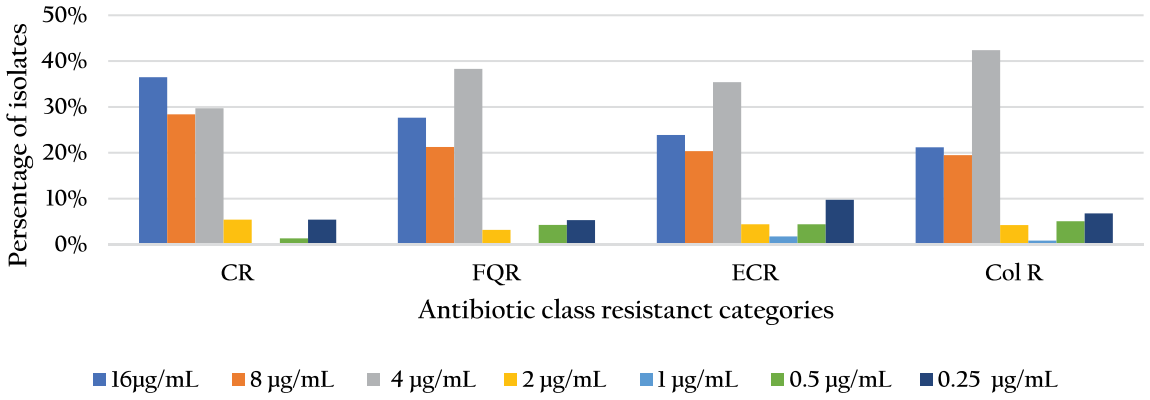

Fig. 10 Minimum inhibitory concentrations of MO-AgNPs across antibiotic class resistant categories

Cytotoxicity assay

Cell viability was determined by MTT assay on a normal mouse liver cell line (BNL). The experiment was performed in triplicate, and the ELISA Reader measured the plate readings. The IC50 of MO-AgNPs was 13.47 µg/mL. ELSA readings with mean and standard deviations and the dose-response curve are shown in Fig. 11. The MTT assay plate and cell viability graph are shown in Figure 4S.

Discussion

Antimicrobial Drug Resistance (AMR) has rapidly escalated globally, leading to the development of containment measures to guide research and development of therapeutics. Standardization of MDR definitions was one of these approaches. The novel MDR categorization approach classifies pathogens based on treatment into Susceptible (S), UDR, and DTR [29] and emphasizes the close monitoring of antibiotic-class resistance categories and reserve antibiotic resistance (Last resort antibiotics). These frameworks underscore the impact of antibiotic resistance on clinical outcomes and treatment choices, serving as a valuable epidemiological tool. It suggests that less effective or more toxic antibacterial agents may need to be considered in therapeutic decision-making, which raises health concerns and contributes to increased antibiotic overuse and infection control costs [14].

Estimates at the species level in the current study revealed that 9 distinct taxon-specific were reported, those species included *Acinetobacter baumannii, Pseudomonas aeruginosa*, and *E. coli.* Those three taxa were ranked as critical on the WHO priority pathogens list for research and development [30], as well as less frequent but clinically distinct Gram-negative taxa, including *Sphingomonas paucimobis, Citrobacter koseri, Serratia marcesens*, and *Salmonella group* which frequently exhibit resistance. Taxa that displayed DTR-resistant phenotypes were *A. baumanni, K. pneumonia, Pseudomonas aeruginosa, Proteus mirabilis, E. coli,* and *Sphingomonas paucimobis*. Even though DTR was uncommon in *E. coli*, it cannot be ignored in *A. baumannii, K. pneumonia, P. aeruginosa*, and *P. mirabilis*. These findings are consistent with results were reported by the epidemic trends in China [18] and in the USA [14].

According to antibiotic-class resistance categorization, *A. baumannii* exhibited the highest CR, FQR, ECR, and Col R resistant patterns, accounting for 86% for each CR, FQR, and Col R, and 100% for ECR, These findings are consistent with reports from China. [14, 18, 29].

For *K. pneumoniae*, ECR, and Col R were the most prevalent resistance antibiotic class categories, accounting for 85 and 80% Col R respectively. These rates were much higher than those detected in China, the United States, and South Korea [14, 18, 29].

ECR was the most prevalent antibiotic class-resistant category for *E. coli*., accounting for 74%, followed by FQR, with a prevalence rate of 49%. These findings are inconsistent with the surveillance results provided in the US, South, and China [14, 18, 29] which indicated that FQR was the most prevalent phenotype in *E.coli* followed by ECR.

For *P. aeruginosa*, Col R was the highest resistance phenotype accounting for 75%, followed by CR accounting for 50%. Other reports from China, the US, and South Korea reported prevalence rates < 30 in these antibiotic class resistance categories [14, 18, 29].

The regional variations in susceptibility patterns may arise from factors such as antibiotic misuse, varying infection control policies, and differences in sanitation practices across regions.

In the biogenic synthesis of MO-AgNPs, the color shift is attributed to a phenomenon called surface plasmon resonance (SPR), involving the oscillation and interaction of electrons between the positive and negative charges on the surface of the nanoparticle. Spectrophotometric measurements allowed a preliminary characterization of the biosynthesized MO-AgNPs. An absorption band around 450 nm was visible in the absorption spectrum, indicating the formation of AgNPs in the reaction. Similar findings

a

AgNps	Raw data			Blank Corrected Data			Viability %				
Conc	1	2	3	1	2	3	1	2	3	Mean	STD
c	1.897	1.823	1.844	1.73	1.656	1.677	100	100	100	100	0
0.01	1.85	1.857	1.806	1.683	1.69	1.639	99.7235	100.138	97.1163	98.9927	1.33754714
0.03	1.81	1.688	1.769	1.643	1.521	1.602	97.3533	90.1244	94.924	94.1339	3.00360164
0.1	1.76	1.754	1.735	1.593	1.587	1.568	94.3907	94.0352	92.9093	93.7784	0.63141882
0.3	1.627	1.642	1.699	1.46	1.475	1.532	86.51	87.3988	90.7762	88.2283	1.83781107
1	1.616	1.618	1.675	1.449	1.451	1.508	85.8582	85.9767	89.3541	87.063	1.62079702
Blank	0.165	0.167	0.169	Blank Average		0.167	Control average		1.68767		

AgNps	Raw data			Blank Corrected Data			Viability %				
Conc	1	2	3	1	2	3	1	2	3	Mean	STD
c	1.897	1.823	1.844	1.72433	1.65033	1.67133	100	100	100	100	0
3	1.617	1.659	1.574	1.44433	1.48633	1.40133	85.87	88.367	83.3135	85.8502	2.06313
10	1.584	1.592	1.5	1.41133	1.41933	1.32733	83.908	84.3837	78.914	82.4019	2.47396
30	0.695	0.639	0.61	0.52233	0.46633	0.43733	31.0543	27.7249	26.0008	28.26	2.09749
100	0.623	0.655	0.616	0.45033	0.48233	0.44333	26.7737	28.6762	26.3575	27.2691	1.00934
300	1.298	1.221	1.21	1.12533	1.04833	1.03733	66.9045	62.3266	61.6726	63.6346	2.32754
Blank	0.171	0.166	0.181	Blank Average		0.17267	Control average		1.682		

b

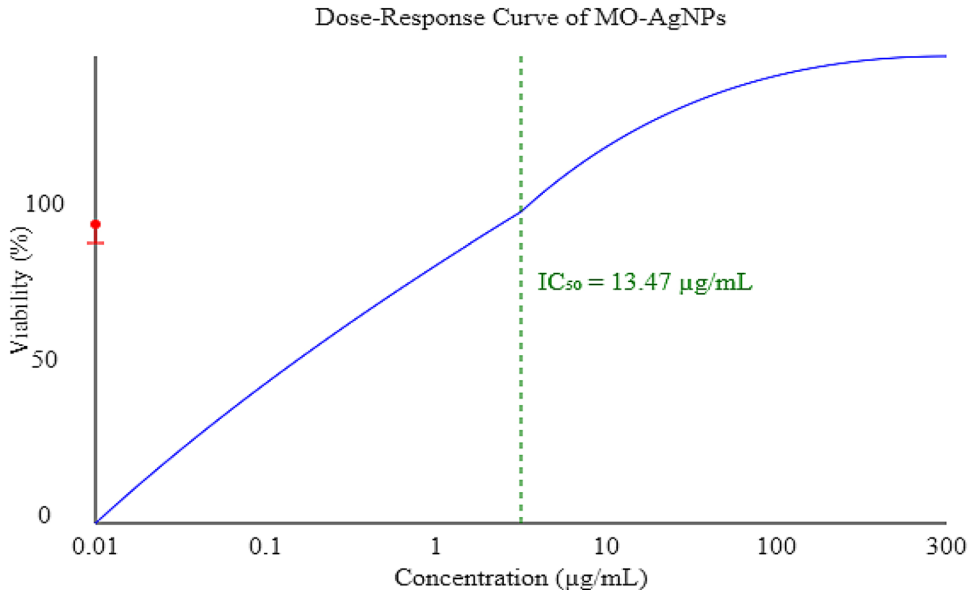

Fig. 11 (**a**) MTT assay results of MO-AgNPs on the BNL cell line and (**b**) the dose response curve

were reported by Haris, in which the absorption band of the synthesized MO-AgNPs was around 440 nm [31].

Three methods, i.e., TEM, SEM, and DLS, were used to determine the size, shape, and hydrodynamic size of MO-AgNPs. The biogenic MO-AgNPs appeared in TEM imaging as spherical nanoparticles (metallic core) with an average size of 12–22 nm, the spherical morphology was confirmed by SEM. A similar study conducted by Asif et al. in which imaging showed uniform MO-AgNPs with globular morphology with an average size of 10–25 nm, larger spherical MO-AgNPs were reported by Ghosh et al. [32], with an average size of 30 nm. The conducted DLS analysis in this study reported a hydrodynamic size of 120 nm, this result aligns with Abdel-Rahman et al. in

which the hydrodynamic size was 100 nm. [19]. The significant disparity between the hydrodynamic diameter (120 nm) and TEM-measured core size (12–19 nm) of MO-AgNPs can be attributed to inherent methodological differences in nanoparticle characterization and interfacial dynamics. TEM analysis reveals the inorganic metallic core under high vacuum conditions, while dynamic light scattering (DLS) accounts for the nanoparticle's effective motion in solution, encompassing phytochemical capping agents (e.g., polyphenols, flavonoids) of *MO* extract form an organic layer around the AgNP core, critical for colloidal stability but undetected in conventional TEM. In addition to the hydration effects, bound water molecules at the nanoparticle-solution interface increase the hydrodynamic radius and Aggregation propensity; the interparticle interactions mediated by surface biomolecules may induce reversible aggregation in solution, disproportionately increasing DLS-derived size measurements. The DLS method, unlike microscopy, does not allow measurement of the size of individual particles within aggregates. Therefore, very often in such cases, the dimensions of the hydrodynamic radius determined by the DLS method are tens of times larger than the dimensions of the particles determined by TEM [33]. SEM images showed some nanoclusters and aggregates in this study.

XRD analysis showed a sharp 2θ angle peak at 37.7, corresponding to the 111 plan, confirming pure AgNPs. These findings were compliant with Asif et al. in which a sharp peak was detected at 38.4 [6]. Moreover, XRD studies specified the crystalline nature of the biosynthesized MO-AgNPs. There were 2θ angle peaks (44°, 64°, and 77°) corresponding to 200, 220, and 311 silver plans, respectively. Furthermore, the dispersed diffraction peaks in the XDR analysis might correspond to the organic compounds stabilizing the exterior of the synthesized MO-AgNPs [6, 31]. The average crystalline size was 12.89 nm, a much smaller crystalline size of 8.05 nm was reported in a previous study [6].

The Zeta potential was −13.7 mV; values between −10 and −30 mV typically indicate moderate stability, suggesting a potential risk of aggregation over time at this level [28]. Low zeta potential values affect reproducibility, often result in variability between batches. Moreover, efficiency might decrease due to instability, impacting their effectiveness.

The EDX spectrum showed the elemental composition of the synthesized MO-AgNPs. EDX pattern showed an Ag signal along with signals of other components C, O, S, N, and Cl [34].

The biogenically synthesized MO-AgNPs demonstrated great antibacterial potential against all the tested pathogens, of different antibiotic class-resistance and resistance phenotypes (S, UDR, and DTR) pathogens. Previous reports demonstrated the antimicrobial potential of MO-AgNPs against both bacteria and fungi [35, 36] and highlighted the efficiency of MO-AgNPs over biogenic AgNPs produced from various plants [37–39].

MO-AgNPs MIC range was 0.25–16 µg/mL across different pathogens, with a MIC/MBC ratio of less than 4 confirming a bactericidal effect on all the tested pathogens. Previous studies conducted on GNB using non-biogenic AgNPs showed higher MIC ranges [24]. Much higher MIC values were reported on using biosynthesized AgNPs from marine *Streptomyces* [40] against GNB. The previous study reported closer MIC values to the current study [41]. The apparent difference in MIC values between the present investigation and the other research could originate from varying sizes, and shapes, as well as the manufacturing process of AgNPs [42].

Nanomaterials, such as AgNPs, have hazardous effects on various organs, including spleen, liver, kidney, and lungs. Therefore, it's crucial to evaluate AgNPs' dynamic in vivo [43–45]. The cytotoxic effect of MO-AgNPs was assessed using an MTT assay on the BNL cell line. Results showed that MO-AgNPs inhibited normal-liver cell growth at IC_{50} 13.47 µg/mL.

On comparing MIC range results to the cytotoxicity results, the reported IC_{50} value of 13.47 µg/mL falls within the MIC range (4–16 µg/mL). Moreover, 40% of isolates scored an MIC of 4 µg/mL, and 80% ($n = 120$) scored an MIC below 16 µg/mL. This means that the MO-AgNPs can effectively kill the pathogenic GNB of different resistance phenotypes at a concentration of ≤ 8 µg/mL, without any damage to normal liver cells.

Overall, the broad-spectrum antimicrobial potential of biogenic MO-AgNPs and their ability to maintain selective toxicity highlight their promise for biomedical applications. Continued research is essential to optimize their properties, elucidate their modes of action, and standardize synthesis and characterization processes for AgNPs. Future Studies should also include combination with different antibiotics along with clinical validation.

While the results are promising, the study has several limitations:

- The zeta potential of −13.3 mV indicates moderate electrostatic stability, suggests that nanoparticles tend to aggregation and precipitation over time, which could alter their antibacterial efficacy, and biodistribution.
- Polydispersity Index (PDI) of 19.4% is considered moderately high for nanoparticle synthesis. This confirms a non-uniform size distribution, meaning there is a wide variety of nanoparticle sizes and aggregates present, aggregation can impact bioavailability, and cellular uptake.

- The cytotoxicity was only tested on a single normal mouse liver cell line (BNL). This does not represent the potential toxicity to other critical cell types, especially human cells.
- Narrow Scope of Antibacterial Testing: The study demonstrates efficacy against a selection of nosocomial pathogens but does not explore efficacy against biofilms & Gram-positive bacteria.

Conclusion

Current research biogenically synthesized AgNPs from MO leave extract. The biogenic MO-AgNPs were spherical with an average size of 12.86 nm and a hydrodynamic size of 120 nm, The polydispersity index was 19.4%, indicating the uniformity of the synthesized particles. and the zeta potential was −13.3 mV reflecting their electrostatic stability in suspension. MO-AgNPs showed a broad spectrum and bactericidal effect against nosocomial pathogens with different Multidrug resistance phenotypes (UDR and DTRs) and different antibiotic class resistance categories, with MIC ≤ 8 µg/mL, against most pathogens and IC_{50} = 13.47 µg/mL against normal mouse liver cell line (BNL). The reported MIC was significantly below the cytotoxic threshold, providing hope for biogenic MO-AgNPs' potential as a green therapeutic option for nosocomial multidrug-resistant GNB.

Supplementary information

The online version contains supplementary material available at https://doi.org/10.1186/s40816-025-00411-3.

Supplementary Material 1

Acknowledgements
Not applicable.

Author contributions
Conceptualization, H.G., M. A. and H.I.Y.; methodology, N. A. M.A. and H. I.Y.; validation, H.G.; formal analysis, N.A., M.A. and H.I.Y; investigation, H.I.Y.; writing— original draft preparation, N.A.; writing—review and editing, M.A. and H.I.Y.; visualization, H. I.Y.; supervision, H. G. All authors have read and agreed to the published version of the manuscript.

Funding
This research work did not receive any funding.

Data availability
No datasets were generated or analysed during the current study.

Declarations

Ethics approval and consent to participate
Not applicable.

Consent for publication
Not applicable.

Competing interests
The authors declare no competing interests.

Received: 26 May 2025 / Accepted: 6 November 2025
Published online: 21 November 2025

References

1. Neill JO. Antimicrobial resistance: tackling a crisis for the health and wealth of nations the review on antimicrobial resistance chaired; 2014.
2. WHO. Global antimicrobial resistance and use surveillance system (glass) report; 2021.
3. Biswas D, Lyngdoh WV, Lanong S, Jane Lyngdoh C, Bhattacharya P, Mary Lyngdoh N. Detection of colistin resistance in gram negative pathogens: a one year cross-sectional study in a tertiary care centre in Northeast India. Int J Med Public Health. 2023;12(4):175–79. https://doi.org/10.5530/ijmedph.2022.4.32.
4. More PR, Pandit S, De Filippis A, Franci G, Mijakovic I, Galdiero M. Silver nanoparticles: bactericidal and mechanistic approach against drug resistant pathogens. Microorganisms. 2023;11(2). https://doi.org/10.3390/microorganisms11020369.
5. Rai M, Yadav A, Gade A. Silver nanoparticles as a new generation of antimicrobials. Biotechnol Adv. 2009;27(1):76–83. https://doi.org/10.1016/j.biotechadv.2008.09.002.
6. Asif M, Yasmin R, Asif R, Ambreen A, Mustafa M, Umbreen S. Green synthesis of silver nanoparticles (AgNps), structural characterization, and their antibacterial potential. Dose Response. 2022;20(1):1–11. https://doi.org/10.1177/15593258221088709.
7. Patil SV, Mohite BV, Marathe KR, Salunkhe NS, Marathe V, Patil VS. Moringa tree, gift of nature: a review on nutritional and industrial potential. Curr Pharmacol Rep. 2022;8(4):262–80. https://doi.org/10.1007/s40495-022-00288-7.
8. Mahmood KT, Mugal T, Ul Haq I. Moringa oleifera: a natural gift-a review. J Pharm Sci Res. 2010;2(11):775–81.
9. Fidrianny I, Kanapa I, Singgih M. Phytochemistry and pharmacology of moringa tree: an overview. Biointerface Res Appl Chem. 2021;11(3):10776–89. https://doi.org/10.33263/BRIAC113.1077610789.
10. Perumalsamy H, Balusamy SR, Sukweenadhi J, Nag S, MubarakAli D, El-Agamy Farh M, et al. A comprehensive review on moringa oleifera nanoparticles: importance of polyphenols in nanoparticle synthesis, nanoparticle efficacy and their applications. J Nanobiotechnol. 2024;22(1):71. https://doi.org/10.1186/s12951-024-02332-8.
11. Lewis JS II, Weinstein MP, Bobenchik AM, Campeau S, Cullen SK, Dingle T, et al. Performance standards for antimicrobial susceptibility testing. 33rd ed. Wayne, Pa: Clinical and Laboratory Standards Institute; 2023. https://cir.nii.ac.jp/crid/1130578271562670753.
12. T, National Centre for Disease Control (NCDC). Broth - microdilution colistin susceptibility test for aerobic gram - negative bacteria standard operating procedure. Stand Oper Proced. 2020;1–18.
13. McDonnell A, Rex JH, Goossens H, Bonten M, Fowler VG, Dane A. Efficient delivery of investigational antibacterial agents via sustainable clinical trial networks. Clin Infect Dis. 2016;63(Suppl 2):S57–59. https://doi.org/10.1093/cid/ciw244.
14. Kadri SS, Adjemian J, Lai YL, Spaulding AB, Ricotta E, Prevots DR, et al. Difficult-to-treat resistance in gram-negative bacteremia at 173 US hospitals: retrospective cohort analysis of prevalence, predictors, and outcome of resistance to all first-line agents. Clin Infect Dis. 2018;67(12):1803–14. https://doi.org/10.1093/cid/ciy378.
15. CDC. Antibiotic resistance patient safety atlas: phenotypic definitions. 2016:1–4. http://www.cdc.gov/hai/surveillance.
16. Bhatia P, Sharma A, Abhilash JG, Anvitha D, Kumar P, Dwivedi VP, et al. Antibacterial activity of medicinal plants against ESKAPE: an update. Heliyon. 2021;7(2):e06310. https://doi.org/10.1016/j.heliyon.2021.e06310.
17. Zhang Z, Sun Z, Tian L. Antimicrobial resistance among pathogens causing bloodstream infections: a multicenter surveillance report over 20 years (1998–2017). Infect Drug Resist. 2022;15:249–60. https://doi.org/10.2147/IDR.S344875.
18. Zhang Z, Tian L. Trends in DTR, CR, ECR, and FQR in four common gram-negative bacteria: a retrospective study from 2013 to 2021. Infect Drug Resist. 2022;15:2625–31. https://doi.org/10.2147/IDR.S365139.
19. Abdel-Rahman LH, Al-Farhan BS, Abou El-Ezz D, Abd–El Sayed MA, Zikry MM, Abu-Dief AM. Green biogenic synthesis of silver nanoparticles using aqueous extract of Moringa oleifera: access to a powerful antimicrobial, anticancer, pesticidal and catalytic agents. J Inorg Organomet Polym Mater. 2022;32(4):1422–35. https://doi.org/10.1007/s10904-021-02186-9.

20. Adhikari A, Lamichhane L, Adhikari A, Gyawali G, Acharya D, Baral ER, et al. Green synthesis of silver nanoparticles using artemisia vulgaris extract and its application toward catalytic and metal-sensing activity. Inorganics. 2022;10(8). https://doi.org/10.3390/inorganics10080113.
21. Warren BE. X-Ray diffraction methods. J Appl Phys. 1941;12(5):375–84.
22. Pecharsky V, Zavalij P. Fundamentals of powder diffraction and structural characterization of materials. SSBM; 2008.
23. Suryanarayana C, Norton M. X-Ray diffraction: a practical approach. New York: SSBM; 2013.
24. Desouky EM, Shalaby MA, Gohar MK, Gerges MA. Evaluation of antibacterial activity of silver nanoparticles against multidrug-resistant gram negative bacilli clinical isolates from Zagazig University Hospitals. Microbes Infect Dis. 2020;1(1):15–23. https://doi.org/10.21608/MID.2020.27148.1003.
25. Mosmann T. Rapid colorimetric assay for cellular growth and survival: application to proliferation and cytotoxicity assays. J Immunological Methods. 1983;65(1–2):55–63. https://doi.org/10.1016/0022-1759(83)90303-4.
26. Sharma SK, Parashar A, Srivastava A. Interpretation of infrared spectra, a practical approach. CRC press; 1999.
27. Silverstein RM, Webster FX, Kiemle DJ. Spectrometric identification of organic compounds. John Wiley & Sons; 2004.
28. Bhattacharjee S. DLS and Zeta potential - what they are and what they are not? J Control Release. 2016;235:337–51. https://doi.org/10.1016/j.jconrel.2016.06.017.
29. Huh K, Chung DR, Ha YE, Ko J-H, Kim S-H, Kim M-J, et al. Impact of difficult-to-treat resistance in gram-negative bacteremia on mortality: retrospective analysis of nationwide surveillance data. 2020;71(9):487–96. https://doi.org/10.1093/cid/ciaa084.
30. Tacconelli E. Global priority list of antibiotic-resistant bacteria to guide research, discovery, and development of new antibiotics. PLoS One. 2018;10(4):1–11. http://www.cdc.gov/drugresistance/threat-report-2013/ and the Public Health Agency of Canada. PLoS One. 2015;10(4):1–11.
31. Haris Z, Ahmad I. Green synthesis of silver nanoparticles using Moringa Oleifera and its efficacy against gram-negative bacteria targeting quorum sensing and biofilms. J Umm Al-Qura Univ Appl Sci. 2023;0123456789. https://doi.org/10.1007/s43994-023-00089-8.
32. Ghosh N, Paul S, Basak P. Silver nanoparticles of Moringa oleifera – green synthesis, characterisation and its antimicrobial efficacy. J Drug Deliv Ther. 2014;42–46. https://doi.org/10.22270/jddt.v0i0.906.
33. Filippov SK, Khusnutdinov R, Murmiliuk A, Inam W, Ya Zakharova L, Zhang H, et al. Dynamic light scattering and transmission electron microscopy in drug delivery: a roadmap for correct characterization of nanoparticles and interpretation of results. Mater Horiz. 2023;10(12):5354–70. https://doi.org/10.1039/d3mh00717k.
34. Ali K, Ahmed B, Dwivedi S, Saquib Q, Al-Khedhairy AA, Musarrat J. Microwave accelerated green synthesis of stable silver nanoparticles with eucalyptus globulus leaf extract and their antibacterial and antibiofilm activity on clinical isolates. PLoS One. 2015;10(7):1–20. https://doi.org/10.1371/journal.pone.0131178.
35. Islam A, Mandal C, Habib A. Antibacterial potential of synthesized silver nanoparticles from leaf extract of Moringa oleifera. J Retailing Adv Biotechnol Exp Ther. 2021;4(1):67–73. https://doi.org/10.5455/jabet.2021.d108.
36. Prasad TNVKV, Elumalai EK. Biofabrication of Ag nanoparticles using Moringa oleifera leaf extract and their antimicrobial activity. Asian Pac J Trop Biomed. 2011;1(6):439–42. https://doi.org/10.1016/S2221-1691(11)60096-8.
37. Logeswari P, Silambarasan S, Abraham J. Synthesis of silver nanoparticles using plants extract and analysis of their antimicrobial property. J Saudi Chem Soc. 2015;19(3):311–17. https://doi.org/10.1016/j.jscs.2012.04.007.
38. Sharma K, Guleria S, Razdan VK. Green synthesis of silver nanoparticles using ocimum gratissimum leaf extract: characterization, antimicrobial activity and toxicity analysis. J Plant Biochem Biotechnol. 2020;29(2):213–24. https://doi.org/10.1007/s13562-019-00522-2.
39. Yugandhar P, Haribabu R, Savithramma N. Synthesis, characterization and antimicrobial properties of green-synthesised silver nanoparticles from stem bark extract of syzygium alternifolium (WT.) Walp. 3 Biotech. 2015;5(6):1031–39. https://doi.org/10.1007/s13205-015-0307-4.
40. Al-Dhabi NA, Mohammed Ghilan AK, Valan Arasu M, Duraipandiyan V. Green biosynthesis of silver nanoparticles produced from marine streptomyces sp. Al-dhabi-89 and their potential applications against wound infection and drug resistant clinical pathogens. J Photochem Photobiol B. 2018;189:176–84. https://doi.org/10.1016/J.JPHOTOBIOL.2018.09.012.
41. Lopez-Carrizales M, Itzel Velasco K, Castillo C, Flores A, Magaña M, Martinez-Castanon GA, et al. In vitro synergism of silver nanoparticles with antibiotics as an alternative treatment in multiresistant uropathogens. Antibiotics. 2018;7(2):1–13. https://doi.org/10.3390/antibiotics7020050.
42. Dong Y, Zhu H, Shen Y, Zhang W, Zhang L. Antibacterial activity of silver nanoparticles of different particle size against vibrio natriegens. PLoS One. 2019;14(9):1–12. https://doi.org/10.1371/journal.pone.0222322.
43. Ferdous Z, Nemmar A. Health impact of silver nanoparticles: a review of the biodistribution and toxicity following various routes of exposure. Int J Mol Sci. 2020;21. https://doi.org/10.3390/ijms21072375.
44. Xuand H, Suslick KS. Water-soluble fluorescent silver nanoclusters. Adv Mater. 2010;22(10):1031–164. https://doi.org/10.1002/adma.200904199.
45. Lansdown ABG. Silver in health care: antimicrobial effects and safety in use. Curr Probl Dermatol. 2006;33:17–34. https://doi.org/10.1159/000093928.

Publisher's Note